

Article

ZnO Nano-Rod Arrays Synthesized with Exposed {0001} Facets and the Investigation of Photocatalytic Activity

Xinying Yang¹, Jin Tian¹, Yang Guo¹, Mengyuan Teng¹, Haixia Liu^{1,*} , Tianduo Li¹, Pingli Lv² and Xuping Wang^{3,*}

¹ Shandong Provincial Key Laboratory of Molecular Engineering, School of Chemistry and Chemical Engineering, Qilu University of Technology (Shandong Academy of Sciences), Jinan 250353, China; yangxy961001@163.com (X.Y.); tj401974696@163.com (J.T.); g1940461346@163.com (Y.G.); 18563829180@163.com (M.T.); litianduo@163.com (T.L.)

² School of Light Industry Science and Engineering, Qilu University of Technology (Shandong Academy of Sciences), Jinan 250353, China; qlgdpl@163.com

³ Advanced Materials Institute, Qilu University of Technology (Shandong Academy of Sciences), Jinan 250353, China

* Correspondence: liuhaixia929@163.com (H.L.); wangxp@sdas.org (X.W.); Tel.: +86-183-5310-8823 (H.L.); +86-0531-82605489 (X.W.)

Abstract: Zinc oxide (ZnO) possesses superior chemical and physical properties so that it can occupy an essential position in the application of nanostructures. In this paper, ZnO nano-rod arrays were synthesized by a simple one-step hydrothermal approach with the assistance of cetyl trimethyl ammonium bromide (CTAB). Exposure of the {0001} facets could be controlled by adjusting the amount of CTAB and the maximum exposure of the {0001} facets of ZnO nanorods is obtained at 1.2 g of CTAB. The photocurrent, EIS, and PL measurements support the facile charge transfer with minimum recombination of the photogenerated excitons of the ZnO nano-rod arrays obtained at 1.2 g of CTAB. Consequently, the obtained ZnO nano-rod arrays at the optimal CTAB of 1.2 g exhibit an excellent photocatalytic degradation rate of 99.7% for rhodamine B (RhB), while the degradation rate of RhB by the ZnO obtained without CTAB is only 35%.

Keywords: ZnO nano-rod arrays; morphology; {0001} facets; photocatalytic activity



Citation: Yang, X.; Tian, J.; Guo, Y.; Teng, M.; Liu, H.; Li, T.; Lv, P.; Wang, X. ZnO Nano-Rod Arrays Synthesized with Exposed {0001} Facets and the Investigation of Photocatalytic Activity. *Crystals* **2021**, *11*, 522. <https://doi.org/10.3390/cryst11050522>

Academic Editor: Nabeen K Shrestha, Kun Zheng, Kezhen Qi, Anna Stepień and Rengaraj Selvaraj

Received: 1 April 2021

Accepted: 2 May 2021

Published: 8 May 2021

Publisher's Note: MDPI stays neutral with regard to jurisdictional claims in published maps and institutional affiliations.



Copyright: © 2021 by the authors. Licensee MDPI, Basel, Switzerland. This article is an open access article distributed under the terms and conditions of the Creative Commons Attribution (CC BY) license (<https://creativecommons.org/licenses/by/4.0/>).

1. Introduction

ZnO is a typical n-type semiconductor with a tremendous free exciton binding energy (~60 meV) and a direct band gap (~3.37 eV), which makes ZnO become an important nanomaterial [1–4]. It is known to us all that ZnO nanostructure possesses excellent optical and electrical properties, gas-sensitivity, good chemical stability, and low toxicity. Indeed, all of the remarkable properties broaden their applications in various aspects, e.g., electro-optical devices, gas sensors, varistors, photocatalysts for photo-splitting of water into hydrogen, and degrading pollutants [5–9]. One of the most promising applications is photodegrading pollutants to protect the environment. The issue of photocatalytic activity has received considerable critical attention, and the photocatalytic performance of ZnO catalysts is closely related to the exposed surfaces of samples. Although the control of morphology has seen much progress in the past few years, it remains the focus of research in the nanotechnology field [10–12].

ZnO nanostructures demonstrate considerable superiority as photocatalysts for degrading pollutants through simple photocatalytic reactions. Since different morphologies of ZnO nanostructures show different optical and electrical properties, people do their best to find the superior fabrication process for ZnO nanostructures with excellent properties. There is evidence that the surfactant plays a crucial role in regulating the morphology of the ZnO nanostructure [13–15]. At present, a variety of ZnO nanostructures have been synthesized via different methods [16]. One of the most attractive methods, namely the

hydrothermal method is based on surfactant assistance. The surfactant plays an important role in controlling the morphology of ZnO nanostructure. Moreover, active cation agents are one of the most widely used surfactants [17]. So, in our study, we adopted a typical cation active agent called CTAB for controlling the morphology of ZnO nanomaterials. Luo et al. reported that ZnO nano-rod arrays exhibited excellent photocatalytic activity for degrading pollutants [18]. Wen et al. prepared ZnO nanostructures with exposed {1000} facets utilizing a solvothermal method, and ZnO nanorods with spires were obtained by adjusting the proportion of the complexing agent [9]. A. Pimentel et al. reported that three different morphologies of ZnO were synthesized by using different solvents and surfactants [19]. However, two or more kinds of surfactants added into the reaction system will increase the difficulty of reaction and the cost of the synthesis process. In addition, the mechanism of ZnO nanostructure makes it more challenging to expound and confirm which reaction path is correct [20–25].

Here, a simple one-step hydrothermal method is used to synthesize ZnO nanorod arrays with exposed {0001} crystal faces. Only one surfactant is added during the entire preparation process. By adjusting the content of CTAB, the morphology of ZnO crystals and the ratio of exposed {0001} crystal faces can be easily controlled. The ammonium salt released by CTAB successfully hindered the nucleation process of ZnO and destroyed the growth direction of the crystal. The photocatalytic test showed that the as-synthesized products exhibited interesting morphology-dependent photocatalytic properties. In addition, a reasonable explanation of the growth mechanism provides a good idea for the design of crystal morphology.

2. Experimental Section

2.1. Materials

The starting materials utilized are zinc nitrate hexahydrate ($\text{Zn}(\text{NO}_3)_2 \cdot 6\text{H}_2\text{O}$, analysis purity grade, Sinopharm Chemical Reagent Co. Ltd., Shanghai, China), cetyl trimethyl ammonium bromide (CTAB, $\text{C}_{19}\text{H}_{42}\text{BrN}$, 99.9%, Shanghai Aladdin Biochemical Technology Co. Ltd., Shanghai, China), sodium hydroxide (NaOH, Tianjin guangfu Technology Development Co. Ltd., Tianjin, China) were used without further purification. Absolute ethanol (Tianjin Fuyu Fine Chemical Co. Ltd., Tianjin, China) was used to wash precipitate followed by reaction progress, and distilled water was used throughout the experiment.

2.2. Synthesis of ZnO Nano-Rod Arrays

In a typical synthesis, 0.749 g zinc nitrate hexahydrate, 0.8 g cetyl trimethyl ammonium bromide and 1.0 g sodium hydroxide were mixed, dissolved in 40 mL distilled water under constant stirring until a homogeneous solution obtained. The obtained solution was introduced into a dried Teflon autoclave (100 mL) and kept at 120 °C for 10 h in an electro-thermostatic blast oven. When the reaction ended, the oven was turned off and cooled down to room temperature, the white precipitate was collected and then washed with absolute ethanol and distilled water several times. After drying in an oven at 60 °C for 22 h. In the experiment, kept the amount of $\text{Zn}(\text{NO}_3)_2 \cdot 6\text{H}_2\text{O}$ and NaOH were invariant and changed the quantity of CTAB (0 g, 1.0 g, 1.2 g, 1.4 g) to obtain ZnO with different morphologies.

2.3. Characterization

The morphology of ZnO nano-rod arrays products was examined by using scanning electron microscopy (SEM, Regulus 8220, Hitachi, Tokyo, Japan). X-Ray diffraction (XRD) patterns were obtained (Rigaku Corp., Tokyo, Japan) by using a Bruker D8 advanced X-ray powder diffractometer with Cu-K α radiation ($\lambda = 1.5418 \text{ \AA}$). The N_2 adsorption and desorption test of samples were measured on a Qutachrome Autorsorb IQ instrument and calculated by the Brunauer-Emmett-Teller (BET) method to obtain the specific surface area (Autorsorb IQ, Quantachrome, Boynton Beach, FL, USA). The UV-vis absorption spectrum was measured by an UV-visible spectrophotometer (UV2600, Shimadzu, Tokyo, Japan). The

photoluminescence (PL) spectrum was measured on a spectrofluorophotometer (F97Pro, Lengguang, Shanghai, China) at room temperature.

2.4. Photocatalytic Activity

ZnO nanomaterials have been widely applied in the photocatalytic degradation of contaminants because of their predominant photocatalytic efficiency and environmental nature. The photocatalytic activity of the as-prepared ZnO nano-rod arrays was evaluated by degradation of rhodamine B (RhB) dye as a model dye under UV-vis light irradiation at room temperature. In a typical experiment, 0.01 g of rhodamine B was dissolved absolutely in a 500 mL beaker and then transferred to a dried 500 mL volumetric flask, diluted to volume, and mixed. Then, 0.1 g of as-prepared ZnO nano-rod arrays produced with different amounts of CTAB was dispersed in a 200-mL glass beaker containing 100 mL RhB (20 mg/L) aqueous solution. The mixture was stirred magnetically in the dark for 30 min to obtain the equilibrium adsorption between the surface of the photocatalyst and RhB molecules. A 300-W Xe arc lamp (PLS-SXE300UV, Beijing Perfectlight Co. Ltd., Beijing, China) served as the light source to provide UV-Vis light. Then, 3 mL of supernatant was obtained every 20 min. This was monitored by UV-Vis spectroscopy (UV-2600, Shimadzu, Tokyo, Japan). After every time UV-vis radiation, the photodegradation of the RhB dye was defined as follows: $\eta = (1 - C/C_0) \times 100\%$, where η is RhB degradation efficiency. C_0 and C represent the initial and final concentration absorbance of RhB dye.

2.5. Photoelectrochemical Measurements

The photocurrent density, EIS and Mott–Schottky was test measured by CHI 760E electrochemical workstation (Shanghai, China). The electrolyte used in the test is 0.5 M Na_2SO_4 aqueous solution. First, ground 20 mg of catalyst with 1 mL of absolute ethanol. Then, we used a spin coater to apply 200 μL of the catalyst evenly on 2×2 cm of clean ITO glass. The prepared samples were dried at 80 °C for 2 h to obtain working electrodes. The light source was obtained from a 300-W Xe lamp (PLS-SXE300UV, Beijing Perfectlight Co. Ltd., Beijing, China). The platinum was used as a counter electrode and Ag/AgCl was used as a reference electrode.

3. Results and Discussion

3.1. Morphology and Structure

XRD and SEM tests were performed to present the structure and morphology of as-prepared ZnO nano-rod arrays. The purity and phase of ZnO nanoparticles were determined by XRD, and the results were shown in Figure 1. It can be seen that all of the diffraction peaks are in agreement with the JCPDS card of ZnO (JCPDS 36-1451), which can be indexed as hexagonal wurtzite phase ZnO nanostructure. It was observed that, as the mass of CTAB increases, the intensity of the (002) peak tends to increase, and no peaks from other structures or impurities were observed, indicating the high purity of the ZnO nano-rods [26]. The sharp diffraction peaks proved that the ZnO products have good crystallinity. In addition, according to the previously reported method [27,28], the crystal structure parameters of all samples were calculated from XRD data, as shown in Table 1. It can be seen that the different contents of CTAB added to the sample leads to subtle changes in the lattice parameters, which are attributed to the influence of internal residual stress. The microstrain value is generally caused by internal stress, so the microstrain changes with the lattice parameters.

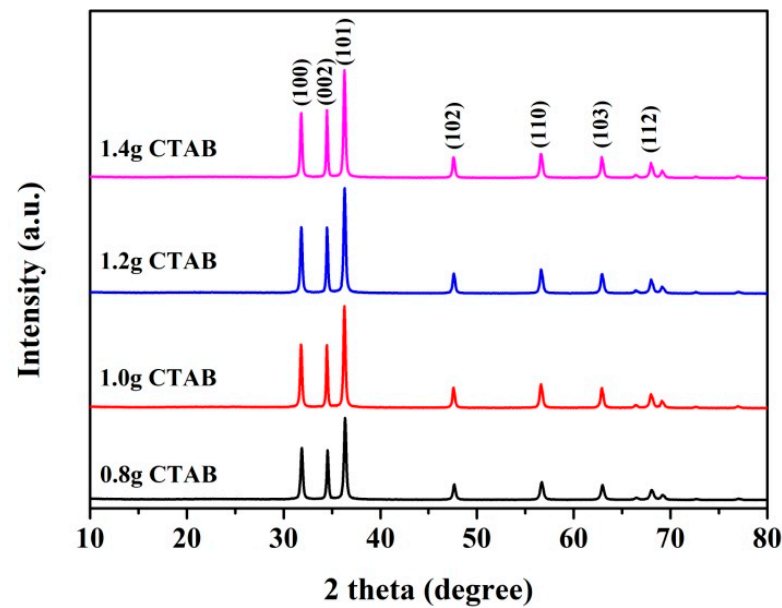


Figure 1. XRD patterns of the as-prepared ZnO synthesized with different quantities of CTAB.

Table 1. Crystal structure parameters of all samples calculated from XRD data.

Sample	Unit Cell Parameter a, Å	Unit Cell Parameter c, Å	Microstrain, %	Grain Size, Å
0.8 g CTAB	3.2421	5.2010	0.161	990
1.0 g CTAB	3.2484	5.2058	0.075	675
1.2 g CTAB	3.2464	5.2043	0.089	651
1.4 g CTAB	3.2476	5.2052	0.072	667

To observe the morphology of ZnO nano-rod arrays. Figure 2 shows SEM micrographs of ZnO nano-rod arrays with different mass of CTAB. When the amount of CTAB was 0.8 g, the gross morphology of ZnO nanostructures was nano-rod arrays as in Figure 2a. It's obvious to see that all rods were with sharp tops in the enlarger images (Figure 2b). All of the nano-rods with an average length of 1.1 μm and a diameter of 100 nm and exhibited a well-regulated emanative nanostructure. It indicates that a self-assembly process could exist during the growth of ZnO nanocrystalline. As shown in Figure 2c,d, the amount of CTAB is 1.0 g, ZnO nano-rods are in the shape of a hexagonal prism and nano-rods with pencil-like tip. The length of ZnO nanorods is about 2.5 μm . These nanorods begin to reunite into flower-like structures. After we added CTAB up to 1.2 g, ZnO nano-rods equipped with a flat top. The ZnO particles exhibited a well-regulated arrangement nanostructure were obtained as shown in Figure 2e,f. The order-oriented ZnO nano-rod arrays with an average length of 1.4 μm and a diameter of 70 nm. When the amount of CTAB was 1.4 g, the morphology of ZnO nanoparticles was hexagonal flakes and aggregates into flower-like structures (Figure 2g,h).

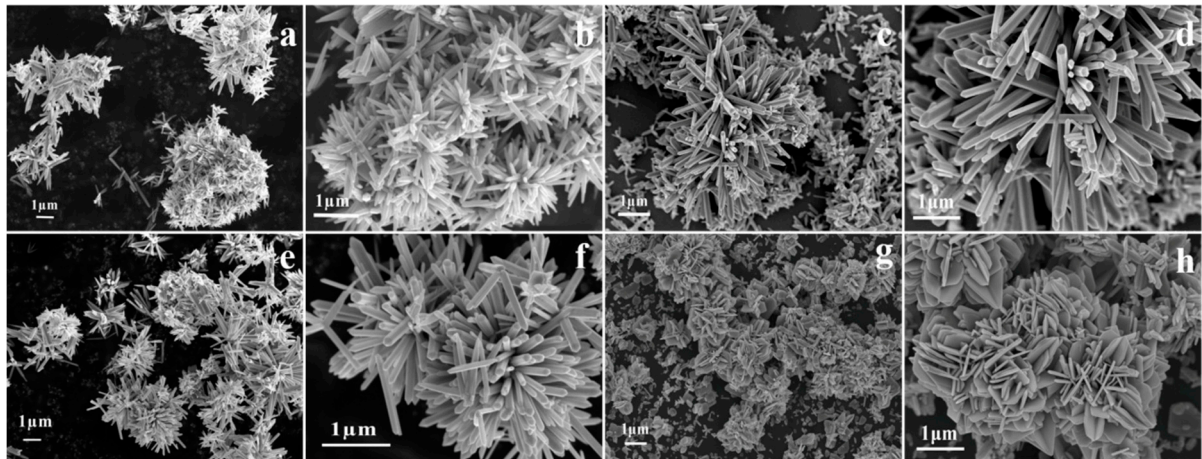


Figure 2. SEM micrographs of ZnO nano-rods: (a,b): 0.8 g CTAB; (c,d): 1.0 g CTAB; (e,f): 1.2 g CTAB and (g,h): 1.4 g CTAB.

3.2. The growth Mechanism of ZnO Nano-Rod Arrays

According to the morphology and phase structure of ZnO nano-rod arrays above, we propose a reasonable growth mechanism of ZnO nanocrystalline (Figure 3). The differences in the morphology of ZnO particles were resulting from the experimental growth conditions, which strongly depends on the amount of CTAB in this study. Normally, in a typical hydrothermal process, compared to the [0001] direction, the speed of crystal growth in other directions will be slower. Therefore, ZnO nanocrystals were easier to form 1-D nanostructures [13,24–26,29]. Supplementary Figure S1 shows the SEM image of ZnO without CTAB and promoters that hinder the nucleation process and disrupt the direction of crystal growth are the main factors affecting morphological changes [13]. According to the previous knowledge, the maximal crystal growth velocity was along the [0001] direction in the hydrothermal synthesis process. The maximal growth velocity is characteristic of the growth in +C direction. Compared with other different directions, there was an interesting relationship between them: $V [10\bar{1}0] < V [01\bar{1}1] < V [01\bar{1}0] < V [0001]$ [19]. Different growth velocities will produce different crystal planes. The surface with faster growth velocities, such as {0001} planes, will continuously reduce the plane ratio, while the surface with slower growth velocities, such as {10 $\bar{1}$ 0} planes, will gradually dominate the crystal morphology of crystal [19]. So, ZnO nano-rods with exposed {1000} facets were usually obtained.

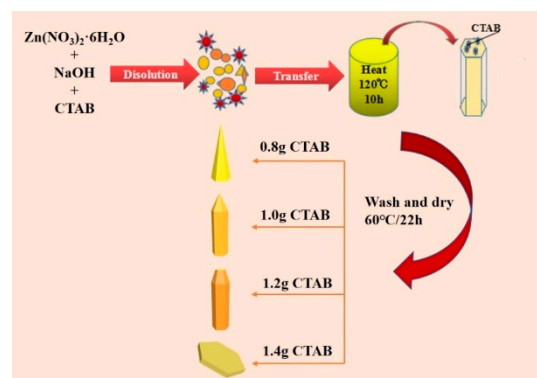
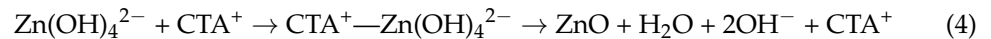
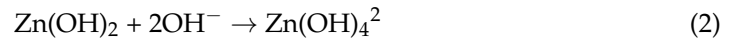
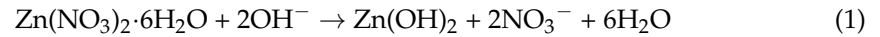


Figure 3. Schematic illustration of the possible formation process for ZnO particles arrays with different amounts of CTAB.

In our synthesis process, NaOH provided OH^- to react with Zn^{2+} to form $\text{Zn}(\text{OH})_4^{2-}$, and CTAB contained ammonium to this reaction system. Due to the lone pair of electrons

on the nitrogen atom, the empty orbitals of the metal particles can react with ammonium to form stable complexes. These complexes can be used as structural units to control the nanostructure of nanocrystals [9,30]. The entire reaction process can be represented by the following equation:



In the initial reaction stage, the Zn^{2+} that supplied from the dissolution of $\text{Zn}(\text{NO}_3)_2 \cdot 6\text{H}_2\text{O}$ reacted with OH^- to form $\text{Zn}(\text{OH})_2$, and then formed $\text{Zn}(\text{OH})_4^{2-}$. The CTA^+ ion ionized by CTAB and $\text{Zn}(\text{OH})_4^{2-}$ ion form a complex $\text{CTA}^+ - \text{Zn}(\text{OH})_4^{2-}$ due to electrostatic interaction [31,32]. As the temperature of the reaction system rises, the complex reacts with the reaction medium and produces ZnO crystals. ZnO as a polar crystal, Zn^{2+} and O^{2-} particles are ordering in a hexagonal close-packed (HCP) pattern, which can be described as each Zn^{2+} lying within a tetrahedral group of four O^{2-} [9]. Although the $\{0001\}$ facets and $\{000\bar{1}\}$ facets of ZnO nanocrystalline have same reticular density, the composition of the outermost atomic layer is different between two facets. The positive charge on the outermost layer of the $\{0001\}$ facets, consisting of zinc ions, while the outermost layer of the $\{000\bar{1}\}$ facets, consisting of oxygen ions. The number of positive charges and negative charges on the different facets is of the same magnitude [13,25]. The ammonium ions released by CTAB in the solvent can be absorbed on the Zn-rich positive plane, thereby reducing the growth rate of the $\{0001\}$ plane. Figure 3 shows the formation process of ZnO nano-rod arrays. Under the low value addition of CTAB reaction condition, dominated growth is along the longitudinal growth direction, which results in the morphology shown in Figure 2a–d. Since the $\{0001\}$ facets had the fastest growth rate and the plane disappears the fastest, resulting in a pointed end of the nano-rods along the +C direction. On the contrary, due to the $\{000\bar{1}\}$ facets with the slowest growth rate, leading to the other end of the nano-rods is planar. With the increase of the amount of CTAB added, the amino complex is adsorbed on the surface of the ZnO crystal nucleus, attached to the $\{0001\}$ facets and inhibited its growth. So, the appearance of flat tops on the nano-rods demonstrates that CTAB successfully restrains the growth of $\{0001\}$ facets, as shown in Figure 2e–f. When adding excess CTAB, $\{0001\}$ facets are covered by the ammonium salt released by CTAB, which inhibits the growth of ZnO crystals in the length direction. Therefore, the $\text{Zn}(\text{OH})_4^{2-}$ growth primitives are more attached to other facets, which leads to anisotropic growth of ZnO crystals, where the lateral growth rate is much greater than the growth rate in the c-axis direction. The morphology of the ZnO crystal becomes a hexagonal flake structure, as shown in Figure 2g–h. Figure 4 showed a schematic diagram of the crystal plane of ZnO nanorods to help better understand the process of active surface exposure.

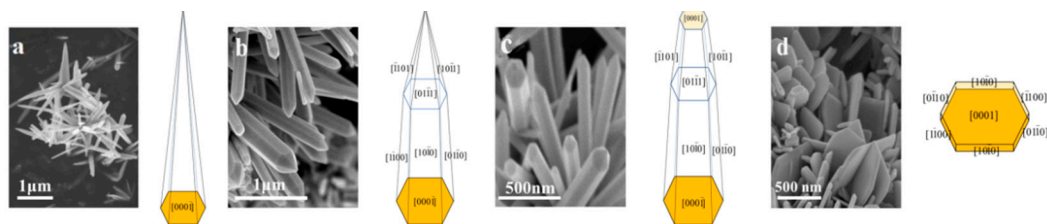


Figure 4. The schematic diagram of ZnO particles arrays with determinate crystal plane: (a): 0.8 g CTAB; (b): 1.0 g CTAB; (c): 1.2 g CTAB; (d): 1.4 g CTAB.

3.3. N₂ Adsorption and Desorption

The specific surface areas and the pore structures usually affect photocatalytic degradation performance. So, the N₂ adsorption and desorption curves were tested (Figure 5 and Supplementary Figure S2) and the specific surface areas were calculated (Table 2). As shown in Figure 5, the N₂ adsorption and desorption curves of all the catalysts are type IV isotherms and the pore diameters are between two and 50 nm, indicating that the catalysts have a mesoporous structure [33]. It can be seen that ZnO without CTAB has the largest specific surface area and pore volume, which is due to the formation of 1-D nanostructures. Without the inhibition of surfactants, ZnO crystals can grow rapidly along the {0001} crystal plane. The specific surface area and pore volume of ZnO prepared with 1.2 g CTAB are larger than other ZnO (with 0.8 g, 1.0 g, 1.4 g CTAB), which is due to the change of morphology caused by the addition of CTAB. The large specific surface area and pore volume are conducive to the adsorption of pollutants by the catalyst, thereby improving the photocatalytic degradation activity [34]. However, the results of ZnO (with 0.8 g and 1.0 g CTAB) are not much different, indicating that the specific surface area and pore volume are not the only factors that affect the photocatalytic activity, and the exposure ratio of the active crystal plane also played an important role in the photocatalytic degradation [35].

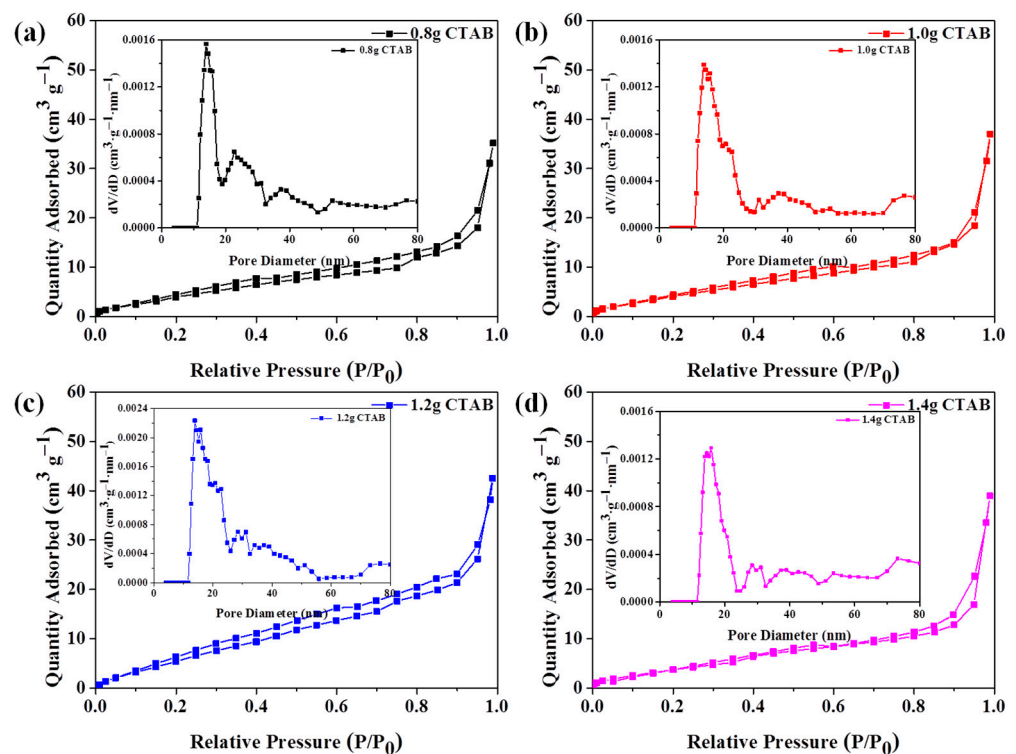


Figure 5. (a–d) N₂ adsorption and desorption and (inset) pore size distribution curves of all samples.

Table 2. BET surface area and pore volume of all samples.

Sample	BET Surface Area (m ² /g)	Pore Volume (cm ³ /g)
0.0 g CTAB	31.9	0.068
0.8 g CTAB	16.2	0.034
1.0 g CTAB	16.6	0.037
1.2 g CTAB	26.4	0.048
1.4 g CTAB	14.8	0.040

3.4. Optical Research of ZnO Nano-Rod Arrays

The optical properties of ZnO samples prepared by adding different amounts of CTAB can be studied through the ultraviolet-visible diffuse reflectance map. All the samples showed obvious absorption in the ultraviolet region, which is mainly caused by the transition of electrons. However, due to its large band gap, there was no absorption in the visible light region [36]. The morphology of ZnO can change the absorption range of ZnO. Therefore, adding different amounts of CTAB will cause the absorption edge of the sample to migrate to different degrees. It can be seen from Figure 6a that, when the addition amount of CTAB is 1.2 g, its absorption range is the largest. In addition, the Kubelka-Munk-transformed reflectance spectra were described to determine the band gap of ZnO with different CTAB amounts [37]. As shown in Figure 6b, when the amount of CTAB added was 1.2 g, the band gap of ZnO was 3.05 eV, which was smaller than the band gap of other CTAB addition amounts of ZnO, indicating that different morphologies can slightly shift the band gap.

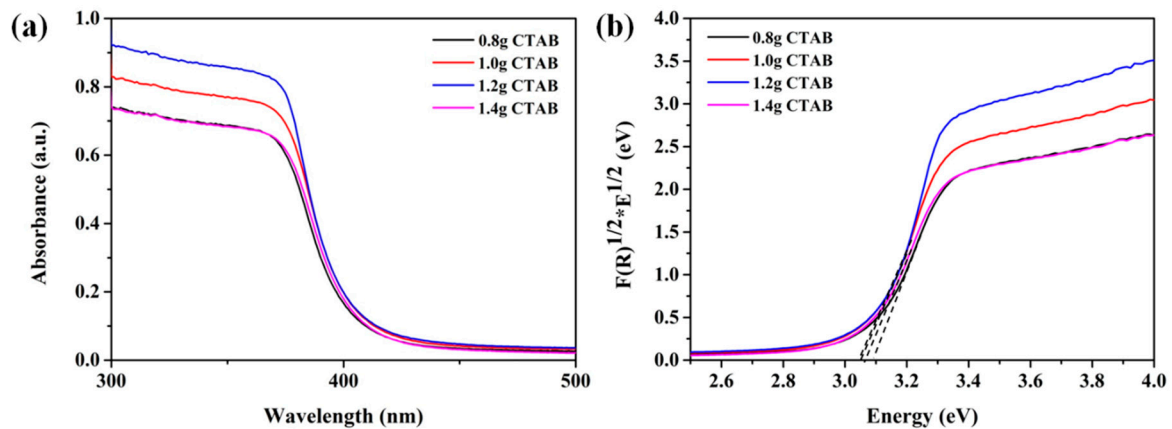


Figure 6. (a) UV-vis absorption spectra of ZnO synthesized with different amounts of CTAB and (b) tauc plot.

The PL spectrum measurement of the prepared ZnO nanorod array was carried out to explore the optical properties. Figure 7 exhibited the PL spectrum among diverse ZnO samples with an excitation wavelength of 325 nm. When the intensity of the light source is greater than the forbidden bandwidth, all of the ZnO samples exhibited a wide PL signal from 400 to 600 nm. Generally speaking, the appearance of the PL peak was attributed to the surface oxygen defects and vacancies of ZnO [38]. At a wavelength of 580 nm, the excited electrons in the conduction band will recombine with the holes left in the valence band, and radiation will occur with the release of energy, which leads to the PL process. The ZnO nano-rod arrays synthesized with 1.2 g CTAB have a higher peak at 580 nm, which indicates that the electron transfer process is relatively rapid, and the energy released in the middle is relatively high. The exposure of the {0001} crystal plane reduces the recombination rate of electrons and holes in the sample, thereby effectively improving the photocatalytic efficiency.

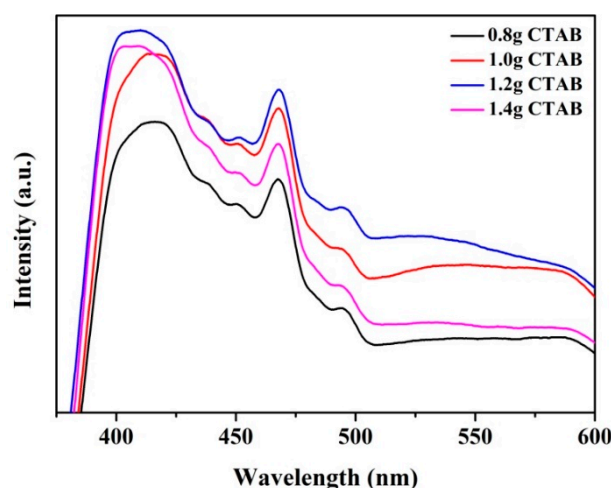


Figure 7. PL spectra for as-prepared ZnO particles arrays at room temperature.

3.5. The Transient Photocurrent Response and EIS Nyquist Plots

To investigate the transfer of photogenerated electrons, the transient photocurrent response curves and EIS Nyquist plots were measured. As shown in Figure 8a, the sample photocurrent intensity is the highest when the amount of CTAB added is 1.2 g. The photocatalytic activity of the catalyst depends on the specific surface area and the exposure of the active surface [36,38]. Due to the exposure of the {0001} facets. The ZnO nano-rods had a higher specific surface area and more active sites. This promotes the separation of photogenerated electrons and holes, thus exhibiting better electrochemical properties. The EIS Nyquist diagram in Figure 8b showed the minimum arc radius of ZnO nano-rod arrays synthesized with 1.2 g CTAB, indicating its small charge transfer resistance [39,40]. Compared to ZnO nano-rod arrays synthesized with 1.2 g CTAB, all ZnO catalysts synthesized with X g CTAB ($X = 0.8, 1.0, 1.4$) showed a larger arc radius, indicating that the addition of 1.2 g CTAB can maximize the exposure of {0001} crystal planes and increase the number of active sites to improve photocatalytic degradation activity, which was consistent with the above analysis results.

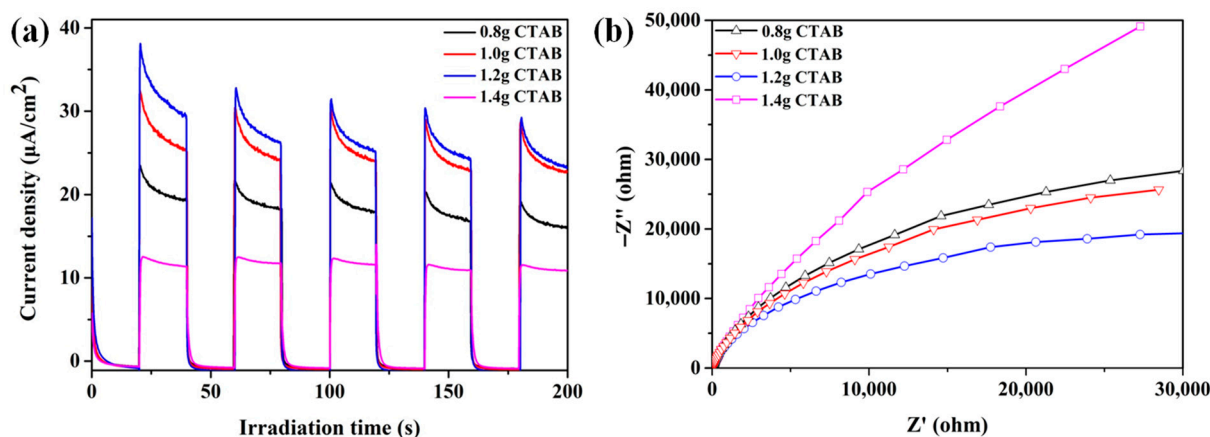


Figure 8. (a) The transient photocurrent response curves and (b) EIS Nyquist plots of ZnO particles synthesized with different amounts of CTAB.

3.6. The Photocatalytic Activity of ZnO Nano-Rod Arrays

The photocatalytic activity of ZnO nanoparticles was evaluated as the degradation of RhB aqueous solution under UV-vis irradiation ($\lambda < 420$ nm). Figure 9a showed the photocatalytic activity among different ZnO samples. The degradation rate of ZnO synthe-

sized without CTAB after 100 min of UV-vis irradiation is only 35%. However, when ZnO nanostructures that synthesized with different amounts of CTAB were added into RhB solution, the results were showing diverse degradation conditions. The ZnO nanostructures synthesized by 1.2 g CTAB show the most significant photocatalytic activity for RhB dye. Figure 9b showed the linear fit between $-\ln(C/C_0)$ and irradiation time among different ZnO samples. It can be more intuitive to see that ZnO nano-rods synthesized with 1.2 g CTAB exhibited the highest photocatalytic activity.

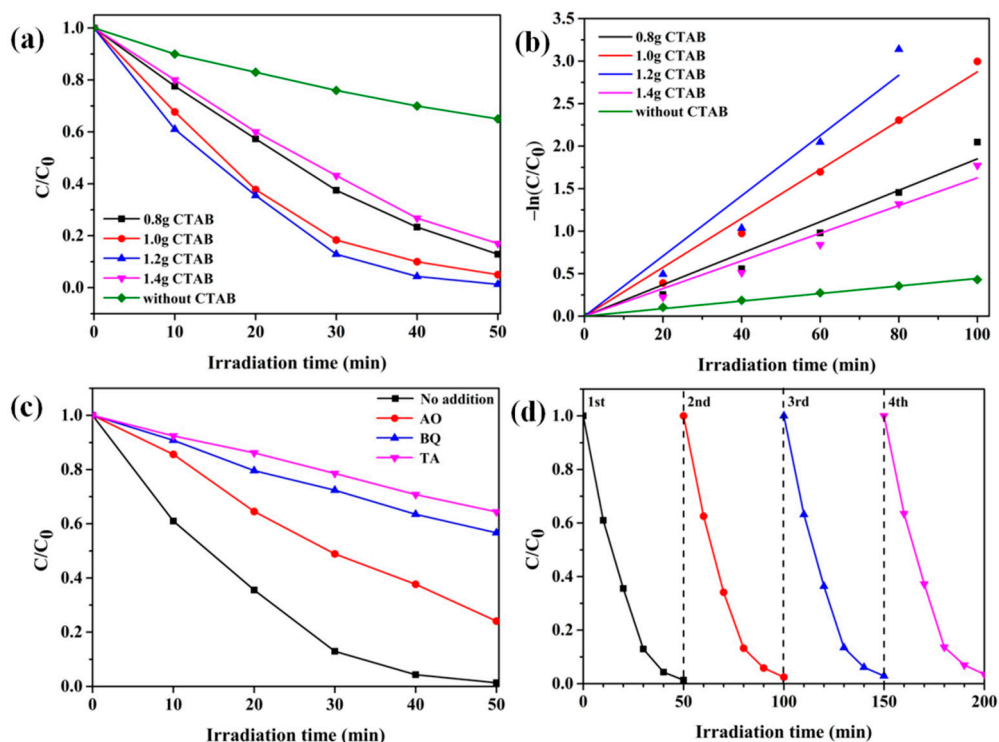


Figure 9. (a) The comparison of photocatalytic activity with different ZnO samples under UV-vis irradiation; (b) linear fit between $-\ln(C/C_0)$ and irradiation time among different ZnO samples; (c) trapping experiments of active species and (d) Cyclic degradation curve of ZnO nano-rod arrays synthesized with 1.2 g CTAB.

The photocatalytic activity is closely related to the active surface exposed to the pollutant area. According to the knowledge of crystallography, the $\{0001\}$ lattice plane is finished in zinc while $\{000\bar{1}\}$ is finished in oxygen. Owing to $\{0001\}$ facets have high surface energy and plentiful active site, which makes it become the most active surfaces of ZnO. In addition, the exposure of $\{0001\}$ facets corresponds to the (0002) diffraction peak on the XRD datum as shown in Figure 1 and the ZnO nanostructure that synthesized by 1.2 g CTAB assisted reaction system exposed more $\{0001\}$ facets (as shown in Figure 4c) compared with 0.8 g CTAB and 1.0 g CTAB assisted reaction system. At the same time, because the ZnO nanorod structure has a higher specific surface area than the nanosheet structure, it may has more active sites on the surface [41]. So, the ZnO nano-rods that exposed $\{0001\}$ facets synthesized with 1.2 g CTAB exhibited excellent photocatalytic activity.

To further study the role of active species in the reaction process, the radical trapping experiments of ZnO nano-rod arrays synthesized with 1.2 g CTAB were carried out (Figure 9c). Compared with no scavenger, it was clearly found that the photocatalytic degradation rate of RhB was significantly decreased after adding BQ or TA, which proved that $\bullet\text{OH}$ and $\bullet\text{O}^{2-}$ play a major role in the photocatalytic activity. In addition, it can be seen that h^+ also affects photocatalytic activity to a certain extent. The recyclability and stability of the ZnO nano-rod arrays synthesized with 1.2 g CTAB were evaluated,

as shown in Figure 9d. Here, it can be seen that the photocatalyst remains at about 97% degradation efficiency after four cycles, indicating it has better potential applications in the wastewater treatment field.

Generally, the conduction band (CB) and valence band (VB) potential of the prepared ZnO determine whether active free radicals can be generated. The Mott-Schottky curve was tested to obtain the flat band potential (E_{fb}), as shown in Figure 10a and Supplementary Figure S3. The E_{fb} of all samples are between 0.44 and 0.48 eV, indicating that the morphology has a weak influence on the flat band potential. For ZnO, it is usually an n-type semiconductor, which can be proved by the positive slope of the tangent line in Figure 10a. It can be seen in the Mott-Schottky plot that the E_{fb} of ZnO was measured to be -0.46 eV (V vs. Ag/AgCl), which was consistent with the of -0.26 eV (V vs. NHE). As we all know, the E_{fb} is approximately equal to the Fermi level (E_F), so, $E_{fb} \approx E_F \approx -0.26$ eV (V vs. NHE) [42]. The conduction band potential of n-type semiconductors is usually 0.2 eV less than the flat band potential [43]. Therefore, the conduction band potential of ZnO is -0.46 eV (V vs. NHE). Due to the band gap of ZnO nano-rod arrays synthesized with 1.2 g CTAB being 3.05 eV, the potential of the VB of ZnO is calculated to be 2.59 eV.

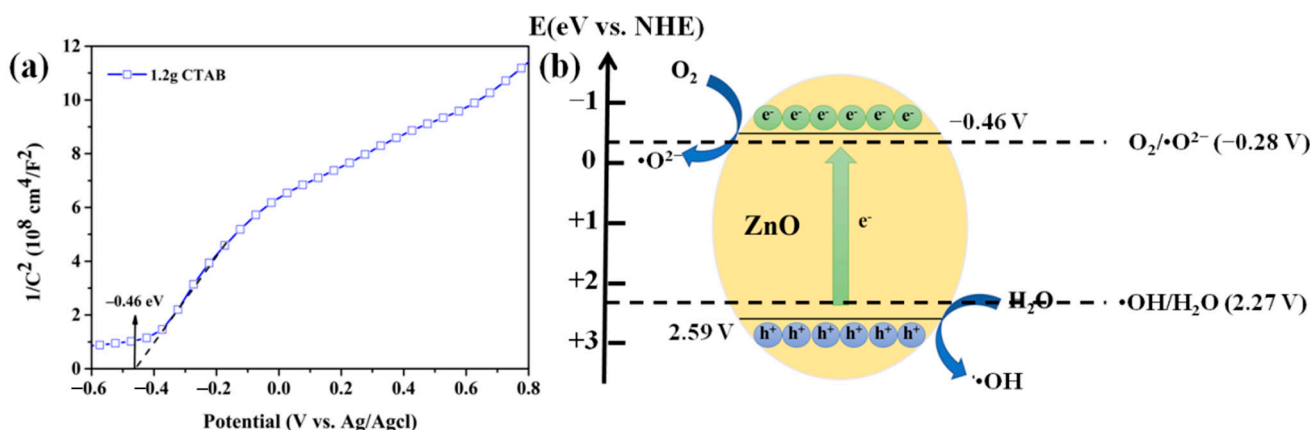


Figure 10. (a) The Mott-Schottky plots and (b) Photocatalytic degradation mechanism of ZnO nano-rod arrays.

As shown in Figure 10b, the photocatalytic degradation mechanism is introduced. When the ZnO surface is irradiated by light with energy greater than or equal to the band gap, electrons (e^-) in the valence band will be excited to the conduction band. Therefore, light-generated holes (h^+) are generated in the valence band. These photo-generated carriers will migrate to the surface of ZnO under the action of electric field. The electrons in the conduction band can react with oxygen on the surface of ZnO to generate superoxide radicals. The holes in the valence band have strong oxidizing properties. They can react with water to form hydroxyl radicals. RhB molecules will react with these free radicals to achieve dye degradation.

4. Conclusions

In conclusion, we have synthesized ZnO nanorod arrays by a CTAB-assisted hydrothermal method. The morphology of ZnO nanostructures changes with the increase of CTAB content, which is due to the ammonium ions released by CTAB in the solvent can be absorbed on the zinc-rich plane, thereby reducing the growth rate of the {0001} plane. When 1.2 g CTAB was added to the reaction system, ZnO nanorods exposed to the {0001} facets were obtained and exhibited excellent photocatalytic performance. The large specific surface area and pore volume are conducive to the adsorption of pollutants by the catalyst and the high exposure ratio of the {0001} facets provided more active sites. Their synergistic effect improves photocatalytic activity. In addition, the cycling tests show that the catalyst has good repeatability and sustainability, indicating that it has better potential applications in the wastewater treatment field.

Supplementary Materials: The following are available online at <https://www.mdpi.com/article/10.3390/cryst11050522/s1>, Figure S1: SEM micrographs of ZnO without CTAB, Figure S2: N₂ adsorption and desorption and (inset) pore size distribution curves of ZnO without CTAB, Figure S3: The Mott-Schottky plots of samples with different contents of CTAB.

Author Contributions: Investigation, X.Y., M.T. and H.L.; methodology, X.Y., T.L. and H.L.; software, X.Y., Y.G. and J.T.; data curation, X.Y. and P.L.; formal analysis, X.Y., J.T. and H.L.; writing—original draft, X.Y. and M.T.; visualization, X.Y., Y.G. and H.L.; writing—review and editing, X.Y., X.W. and H.L.; conceptualization, H.L., X.W.; resources, H.L.; supervision, H.L.; project administration, H.L. and T.L.; funding acquisition, H.L. and T.L. All authors have read and agreed to the published version of the manuscript.

Funding: This work was supported by the financial supports of Natural Science Foundation of Shandong Province(ZR2020ME043), the Key Research Project of Shandong Province (No. 2017GGX40121), the Scientific Research Innovation Team in Colleges and Universities of Shandong Province.

Data Availability Statement: Not applicable.

Conflicts of Interest: The authors declare no conflict of interest.

References

1. Wen, J.; Shi, E.W.; Zhong, W.Z.; Yin, Z.W. growth mechanism and growth habit of oxide crystals. *J. Cryst. Growth* **1999**, *203*, 186–196.
2. Xia, Y.; Wang, J.; Chen, R.S.; Zhou, D.L.; Xiang, L. A Review on the Fabrication of Hierarchical ZnO Nanostructures for Photocatalysis Application. *Crystals* **2016**, *6*, 148. [[CrossRef](#)]
3. Zhang, F.; Li, Y.H.; Qi, M.Y.; Tang, Z.R.; Xu, Y.J. Boosting the activity and stability of Ag-Cu₂O/ZnO nanorods for photocatalytic CO₂ reduction. *Appl. Catal. B Environ.* **2019**, *268*, 118380. [[CrossRef](#)]
4. Nandi, P.; Das, D. Photocatalytic degradation of rhodamine-B dye by stable ZnO nanostructures with different calcination temperature induced defects. *Appl. Surf. Sci.* **2018**, *465*, 546–556. [[CrossRef](#)]
5. Guo, Q.; Fu, L.; Yan, T.; Tian, W.; Wang, X. Improved photocatalytic activity of porous ZnO nanosheets by thermal deposition graphene-like g-C₃N₄ for CO₂ reduction with H₂O vapor. *Appl. Surf. Sci.* **2019**, *509*, 144773. [[CrossRef](#)]
6. Chen, Z.L.; Luo, Y.Y.; Huang, C.X.; Shen, X.T. In situ assembly of ZnO/graphene oxide on synthetic molecular receptors: Towards selective photoreduction of Cr(VI) via interfacial synergistic catalysis. *Chem. Eng. J.* **2021**, *414*, 128914. [[CrossRef](#)]
7. Dodd, A.C.; Mckinley, A.J.; Saunders, M.; Tsuzuki, T. Effect of particle size on the photocatalytic activity of nanoparticulate zinc oxide. *J. Nanopart. Res.* **2006**, *8*, 43–51. [[CrossRef](#)]
8. Rezapour, M.; Talebian, N. Comparison of structural, optical properties and photocatalytic activity of ZnO with different morphologies: Effect of synthesis methods and reaction media. *Mater. Chem. Phys.* **2011**, *129*, 249–255. [[CrossRef](#)]
9. Wen, B.M.; Huang, Y.Z.; Boland, J.J. Controllable growth of ZnO nanostructures by a simple solvothermal process. *J. Phys. Chem. C* **2008**, *112*, 106–111. [[CrossRef](#)]
10. Talebian, N.; Amininezhad, S.M.; Doudi, M. Controllable synthesis of ZnO nanoparticles and their morphology-dependent antibacterial and optical properties. *J. Photochem. Photobiol. B* **2013**, *120*, 66–73. [[CrossRef](#)] [[PubMed](#)]
11. Feng, W.L.; Huang, P.; Wang, B.C.; Wang, C.W.; Wang, W.G.; Wang, T.L.; Chen, S.F.; Lv, R.L.; Qin, Y.H.; Ma, J.Y. Solvothermal synthesis of ZnO with different morphologies in dimethylacetamide media. *Ceram. Int.* **2016**, *42*, 2250–2256. [[CrossRef](#)]
12. Gao, H.Y.; Yan, F.W.; Zhang, Y.; Li, J.M.; Zeng, Y.P. Synthesis and characterization of ZnO nanoflowers grown on AlN film by solution deposition. *Chin. Phys. Lett.* **2008**, *25*, 640–643.
13. Pimentel, A.; Nunes, D.; Duarte, P.; Rodrigues, J.; Costa, F.M.; Montero, T.; Martins, R.; Fortunato, E. Synthesis of long ZnO nanorods under microwave irradiation or conventional heating. *J. Phys. Chem. C* **2014**, *118*, 14629–14639. [[CrossRef](#)]
14. Pascariu, P.; Olaru, N.; Rotaru, A.; Airinei, A. Innovative low-cost carbon/ZnO hybrid materials with enhanced photocatalytic activity towards organic pollutant dyes removal. *Nanomaterials* **2020**, *10*, 1873. [[CrossRef](#)]
15. Luo, S.R.; Chen, R.S.; Xiang, L.; Wang, J. Hydrothermal synthesis of (001) facet highly exposed ZnO plates: A new insight into the effect of citrate. *Crystals* **2019**, *9*, 552. [[CrossRef](#)]
16. Wojnarowicz, J.; Chudoba, T.; Lojkowski, W. A review of microwave synthesis of zinc oxide nanomaterials: Reactants, process parameters and morphologies. *Nanomaterials* **2020**, *10*, 1086. [[CrossRef](#)] [[PubMed](#)]
17. Wahab, R.; Ansari, S.G.; Kim, Y.S.; Song, M.W.; Shin, H.S. The role of pH variation on the growth of zinc oxide nanostructures. *Appl. Surf. Sci.* **2009**, *255*, 4891–4896. [[CrossRef](#)]
18. Luo, S.; Liu, C.W.; Li, W.; Liu, S.X.; He, S.B. Self-assembly of single-crystal ZnO nanorod arrays on flexible activated carbon fibers substrates and the superior photocatalytic degradation activity. *Appl. Surf. Sci.* **2020**, *513*, 145878. [[CrossRef](#)]
19. Pimentel, A.; Rodrigues, I.; Duarte, P.; Nunes, D.; Costa, F.M.; Montetiro, T.; Martins, R.; Fortunato, E. Effect of solvents on ZnO nanostructures synthesized by solvothermal method assisted by microwave radiation: A photocatalytic study. *J. Mater. Sci.* **2015**, *50*, 5777–5787. [[CrossRef](#)]

20. Demyanets, L.N.; Li, L.E.; Uvarova, T.F. Zinc oxide: Hydrothermal growth of nano and bulk crystals and their luminescent properties. *J. Mater. Sci.* **2006**, *41*, 1439–1444. [[CrossRef](#)]
21. Gomez, J.L.; Tigli, O. Zinc oxide nanostructures: From growth to application. *J. Mater. Sci.* **2013**, *48*, 612–624. [[CrossRef](#)]
22. Xia, W.; Wang, Y.; Wang, Q.; Yan, Y.Z.; Jiang, Y.J. Tubular acceptor-rich ZnO hierarchical heterostructure as an efficient photocatalyst for organic degradation. *Appl. Surf. Sci.* **2020**, *506*, 145008. [[CrossRef](#)]
23. Lu, H.; Deng, K.M.; Shi, Z.W.; Liu, Q.; Zhu, g.B.; Fan, H.T.; Li, L. Novel ZnO microflowers on nanorod arrays: Local dissolution-driven growth and enhanced light harvesting in dye-sensitized solar cells. *Nanoscale Res. Lett.* **2014**, *9*, 183–191. [[CrossRef](#)]
24. Alenezi, M.R.; Alshammari, A.S.; Jayawardena, K.; Beliatis, M.J.; Henley, S.J.; Silva, S.R.P. Role of the exposed polar facets in the performance of thermally and UV activated ZnO nanostructured gas sensors. *J. Phys. Chem. C* **2013**, *117*, 17850–17858. [[CrossRef](#)]
25. Zhou, X.; Xie, Z.X.; Jiang, Z.Y.; Kuang, Q.; Zhang, S.H.; Xu, T.; Huang, R.B.; Zheng, L.S. Formation of ZnO hexagonal micropyrramids: A successful control of the exposed polar surfaces with the assistance of anionic liquid. *Chem. Commun.* **2005**, *28*, 5572–5574. [[CrossRef](#)] [[PubMed](#)]
26. Sarkar, D.; Tikku, S.; Thapar, V.; Srinivasa, R.S.; Khilar, K.C. Formation of zinc oxide nanoparticles of different shapes in water in-oil microemulsion. *Colloids Surface A* **2011**, *381*, 123–129. [[CrossRef](#)]
27. Trukhanov, A.V.; Darwish, K.A.; Salem, M.M.; Hemeda, O.M.; Trukhanov, S.V. Impact of the heat treatment conditions on crystal structure, morphology and magnetic properties eVolution in BaM nanohexaferrites. *J. Alloys Compd.* **2021**, *866*, 158961. [[CrossRef](#)]
28. Zubar, T.I.; Fedosyuk, V.M.; Trukhanov, A.V.; Kovaleva, N.N.; Tishkevich, D.I. Control of growth Mechanism of Electrodeposited Nanocrystalline NiFe Films. *J. Electrochem. Soc.* **2019**, *166*, D173–D180. [[CrossRef](#)]
29. Gomez, H.; Dalchiele, E.A.; Martti, R.E. Morphological and structural control of electrodeposited ZnO thin films and its influence on the photocatalytic degradation of methyl orange dye. *Int. J. Electrochem. Sci.* **2014**, *9*, 534–548.
30. Mo, M.S.; Yu, J.C.; Zhang, L.Z.; Li, S.A. Self-assembly of ZnO nanorods and nanosheets into hollow microhemispheres and microspheres. *Adv. Mater.* **2005**, *17*, 756–760. [[CrossRef](#)]
31. Wu, C.; Qiao, X.; Chen, J.; Wang, H.; Tan, F.; Li, S. A novel chemical route to prepare ZnO nanoparticles. *Mater. Lett.* **2006**, *60*, 1828–1832. [[CrossRef](#)]
32. Hou, Z.Q.; Wang, Y.X.; Shen, L.H.; guo, H.; Wang, g.C.; Li, Y.; Zhou, S.F.; Zhang, Q.Q.; Jiang, Q. Synthesis of dumbbell-like ZnO microcrystals via a simple solution route. *Nanoscale Res. Lett.* **2012**, *7*, 507–514. [[CrossRef](#)] [[PubMed](#)]
33. Zhang, R.; Zeng, K.L. A novel flower-like dual Z-scheme BiSI/Bi₂WO₆/g-C₃N₄ photocatalyst has excellent photocatalytic activity for the degradation of organic pollutants under visible light. *Diam. Relat. Mater.* **2021**, *115*, 108343. [[CrossRef](#)]
34. Zhang, H.Y.; Li, W.C.; Yan, Y.T.; Wang, W.; Ren, Y.P.; Li, X.W. Synthesis of highly porous g-C₃N₄ nanotubes for efficient photocatalytic degradation of sulfamethoxazole. *Mater. Today Commun.* **2021**, *27*, 102288. [[CrossRef](#)]
35. Kusiak-Nejman, E.; Wojnarowicz, J.; Morawski, A.W.; Narkiewicz, U.; Sobczak, K.; gierlotka, S.; Lojkowski, W. Size-dependent effects of ZnO nanoparticles on the photocatalytic degradation of phenol in a water solution. *Appl. Surf. Sci.* **2021**, *541*, 148416. [[CrossRef](#)]
36. Yang, X.Y.; Liu, H.X.; Li, T.D.; Huang, B.B.; Hu, W.; Jiang, Z.Y.; Chen, J.B.; Niu, Q.F. Preparation of flower-like ZnO@ZnS core-shell structure enhances photocatalytic hydrogen production. *Int. J. Hydrog. Energy* **2020**, *45*, 26967–26978. [[CrossRef](#)]
37. Li, X.; He, W.M.; Li, C.H.; Song, B.; Liu, S.W. Synergetic surface modulation of ZnO/Pt@ZIF-8 hybrid nanorods for enhanced photocatalytic CO₂ valorization. *Appl. Catal. B Environ.* **2021**, *287*, 119934. [[CrossRef](#)]
38. Liu, Y.J.; Huang, D.; Liu, H.X.; Li, T.D.; Wang, J.G. ZnO tetrakaidecahedrons with coexposed {001}, {101}, and {100} facets: Shape-selective synthesis and enhancing photocatalytic performance. *Cryst. Growth Des.* **2019**, *19*, 2758–2764. [[CrossRef](#)]
39. Hao, X.Q.; Zhou, J.; Cui, Z.W.; Wang, Y.C.; Wang, Y.; Zou, Z.G. Zn-vacancy mediated electron-hole separation in ZnS/g-C₃N₄ heterojunction for efficient visible-light photocatalytic hydrogen production. *Appl. Catal. B Environ.* **2018**, *229*, 41–51. [[CrossRef](#)]
40. Chen, Z.; Fan, T.T.; Yu, X.; Wu, Q.L.; Zhu, Q.H.; Zhang, L.Z.; Yi, X.D. gradual carbon doping of graphitic carbon nitride towards metal-free visible light photocatalytic hydrogen eVolution. *J. Mater. Chem. A* **2018**, *6*, 15310–15319. [[CrossRef](#)]
41. Bai, S.L.; Liu, X.; Li, D.Q.; Chen, S.; Luo, R.X.; Chen, A.F. Synthesis of ZnO nanorods and its application in NO₂ sensors. *Sens. Actuat. B Chem.* **2011**, *153*, 110–116. [[CrossRef](#)]
42. Liang, H.Q.; Tai, X.M.; Du, Z.P.; Yin, Y.J. Enhanced photocatalytic activity of ZnO sensitized by carbon quantum dots and application in phenol wastewater. *Opt. Mater.* **2020**, *100*, 109674. [[CrossRef](#)]
43. Ren, C.J.; Li, W.J.; Li, H.D.; Ma, X.H.; Li, X.Y.; Fan, H.X.; Chen, Y.Y. Fabrication of chrysanthemum-like CdSe/bulk WC: A novel Schottky-junction photocatalyst for improving photocatalytic hydrogen production. *J. Alloys Compd.* **2021**, 159691. [[CrossRef](#)]